DR. YUANHE YANG (Orcid ID : 0000-0002-5399-4606)

Article type : Primary Research Articles

Title: Permafrost nitrogen status and its determinants on the Tibetan Plateau

Running head: Permafrost N pools and transformation rates

Chao Mao[1,2], Dan Kou[1,3], Leiyi Chen[1], Shuqi Qin[1,2],
Dianye Zhang[1,2], Yunfeng Peng[1], and Yuanhe Yang[1,2*]

[1]State Key Laboratory of Vegetation and Environmental Change, Institute of Botany, Chinese Academy of Sciences, Beijing 100093, China

[2]University of Chinese Academy of Sciences, Beijing 100049, China

[3]Biogeochemistry Research Group, Department of Biological and Environmental Sciences, University of Eastern Finland, Kuopio, Finland

[*]**Corresponding author:** Dr. Yuanhe Yang, tel.: + 86 10-6283 6638, fax: + 86 10-6283 6632, E-mail: yhyang@ibcas.ac.cn

Revised manuscript submitted to *Global Change Biology*

1st-June-2020

Manuscript information: 48 pages, 6 figures, 1 supplementary text, 4 supplementary tables, and 12 supplementary figures.

Abstract

It had been suggested that permafrost thaw could promote frozen nitrogen (N) release and modify microbial N transformation rates, which might alter soil N availability and then regulate ecosystem functions. However, the current understanding of this issue is confined to limited observations in the Arctic permafrost region, without any systematic measurements in other permafrost regions. Based on a large-scale field investigation along a 1000-km transect and a laboratory incubation experiment with a ^{15}N pool dilution approach, this study provides the comprehensive evaluation of the permafrost N status, including the available N content and related N transformation rates, across the Tibetan alpine permafrost region. In contrast to the prevailing view, our results showed that the Tibetan alpine permafrost had lower available N content and net N mineralization rate than the active layer. Moreover, the permafrost had lower gross rates of N mineralization, microbial immobilization and nitrification than the active layer. Our results also revealed that the dominant drivers of the gross N mineralization and microbial immobilization rates differed between the permafrost and the active layer, with these rates being determined by microbial properties in the permafrost while regulated by soil moisture in the active layer. In contrast, soil gross nitrification rate was consistently modulated by the soil NH_4^+ content in both the permafrost and the active layer. Overall, patterns and drivers of permafrost N pools and transformation rates observed in this study offer new insights into the potential N release upon permafrost thaw and provide important clues for Earth system models to better predict permafrost biogeochemical cycles under a warming climate.

Key words: climate warming, permafrost thaw, frozen nitrogen, nitrogen availability, nitrogen cycle, nitrogen transformation rates

Introduction

Permafrost underlies approximately 24% of the land area of the Northern Hemisphere (Zhang, Barry, Knowles, Heginbottom, & Brown, 1999). Over the past decades, climate warming has occurred continuously in permafrost regions (Biskaborn et al., 2019; Hu et al., 2019), with global permafrost temperature increasing by about 0.3 °C decade^{-1} (Biskaborn et al., 2019). The warming climate has induced widespread permafrost thaw (Chadburn et al., 2017; Ran, Li, & Cheng, 2018), which may trigger considerable amounts of permafrost nitrogen (N) release (Finger et al., 2016; Salmon et al., 2016) and further induce two ecological consequences. For one thing, the increased soil N availability could facilitate plant N uptake and enhance ecosystem production (Keuper et al., 2017; Salmon et al., 2016). For another, the elevated soil available N content could be prone to the N removal via hydrologic export (Harms & Jones, 2012; Wickland et al., 2018) and nitrous oxide (N_2O) emissions through nitrification and denitrification processes (Voigt et al., 2017; Yang et al., 2018). A better understanding of soil N release upon permafrost thaw and its underlying drivers is thus important for predicting the fate of these deeper soil N pools and their effects on ecosystem function in permafrost-affected regions.

Considering the vital importance of soil N availability to ecosystem function, the global change research community is increasingly concerned with permafrost N release. Current studies have focused on two key parameters, *i.e.*, the frozen available N content and the soil N transformation rates in the thawed permafrost. The former indicates the amount of readily available N in thawing permafrost, while the latter reflects the release of available N from permafrost via microbial N mineralization (Keuper et al., 2012). It has been reported that the dissolved inorganic N (DIN) and organic N (DON) content in permafrost are about seven to ten and two times higher than those in the active layer, respectively (Beermann et al., 2017; Harden et al., 2012; Keuper et al., 2012; Salmon et al., 2018). It has also been suggested that the thawed permafrost has higher soil net N mineralization rate than the active layer (Keuper et al., 2012). Taken together, these studies demonstrated that permafrost thaw could result in releasing large amounts of available N (Salmon et al., 2016).

Despite growing attentions on permafrost N release, our understanding is still limited by the following two aspects. First, prior studies mostly focused on the difference in the soil N transformation rates between the permanently frozen soil (permafrost) and seasonally thawed soil (active layer) (*e.g.*, Keuper et al., 2012); however, it remains unclear whether the dominant drivers of N transformation rates vary between the two soil layers. Given that soil physiochemical and microbial properties differ between the permafrost and the active layer (Treat et al., 2014; Waldrop et al., 2010), soil N transformation rates in these two soil layers may be modulated by different variables. Specifically, soil organic matter in the permafrost may exhibit higher decomposability than that in the active layer (Chen et al., 2016; Waldrop et al., 2010) because of the large amounts of labile substrate stored in the deep sediment (Vonk et al., 2015; Wickland et al., 2018). On the contrary, permafrost microorganisms usually show lower abundance and activity than those in the active layer due to the constant low-temperature conditions (Jansson & Taş, 2014). These differences in substrate and microbial properties may result in different drivers for soil N transformation rates between the permafrost and the active layer. However, this question remains unsolved due to the lack of systematic observations at the regional scale.

Second, previous studies were mainly confined to the Arctic permafrost region (*e.g.*, Beermann et al., 2017; Keuper et al., 2012; Salmon et al., 2018), with significant knowledge gaps about other permafrost zones. The Tibetan Plateau, the largest alpine permafrost area, accounts for about 75% of the alpine permafrost region of the Northern Hemisphere (Wang & French, 1995). During the past decades, climate warming has triggered widespread permafrost thaw in this region (Ran et al., 2018), which may have also induced large amounts of soil available N release, as reported in the Arctic region (Salmon et al., 2016). However, the permafrost on the plateau differs from that in the Arctic in several respects, which may lead to different permafrost N status between these two permafrost regions. Compared with the Arctic, the plateau is characterized by a lower soil N density (N stock per area; Harden et al., 2012; Kou et al., 2019) and a deeper active layer thickness (Aalto, Karjalainen, Hjort, & Luoto, 2018; Zhao & Sheng, 2019). The ice content also differs

between the two regions, with less ice in the Tibetan alpine permafrost (Zhang et al., 1999) due to its arid climate with large evaporation under high solar radiation conditions (Yang, Nelson, Shiklomanov, Guo, & Wan, 2010). These distinct conditions suggest that permafrost N status on the plateau may differ from that observed in the Arctic (Beermann et al., 2017; Keuper et al., 2012; Salmon et al., 2018; Wild et al., 2013). However, this issue has not yet been addressed since current studies across the Tibetan alpine permafrost region are confined to the active layer (Chen et al., 2018; Kou et al., 2018; Mao et al., 2019) or the site level (Mu et al., 2015).

In this study, we conducted a large-scale field sampling campaign on the Tibetan Plateau in 2016, and investigated 24 sites across this alpine permafrost region. Based on this field investigation, we measured soil available N content in both the permafrost and the active layer, including the inorganic (NH_4^+ and NO_3^-) and organic (DON) forms, both of which were important N sources for alpine plants on the Tibetan Plateau (Wang et al., 2012; Xu et al., 2011). We also determined soil net and gross N transformation rates, and the associated biotic and abiotic drivers in the two soil layers. By conducting these measurements, we aimed to address the following three questions: (i) Does the permafrost have higher available N content than the active layer? (ii) Does the thawed permafrost have higher rates of net and gross N transformation than the active layer? (iii) Do the dominant drivers of soil N transformation rates differ between the permafrost and active layer?

Materials and Methods

Study area

This study was conducted in representative permafrost regions on the Tibetan Plateau, mainly across the eastern, northeastern and middle parts of the plateau (32.6-38.6 °N, 91.9-99.5 °E; Figure S1), with the average altitude being more than 4000 m. The mean annual temperature varies from -4.5 to 1.8 °C, the mean annual precipitation ranges between 244.6 and 504.2 mm, and the aridity index changes from 0.2 to 0.7 across the study area. This study region, in general, is warmer and drier than most of the permafrost areas in the Arctic (Figure S2). The dominant vegetation types include alpine steppe, alpine meadow and swamp meadow, with the

corresponding dominant species among the three grassland types being *Stipa purpurea* and *Carex moorcroftii*; *Kobresia pygmaea* and *K. humilis*; and *K. tibetica*, respectively (Zhang, Wang, Chen, Li, & Zhao, 1988). The main soil type is Inceptisol (Soil Taxonomy; USDA, 1999) or Cambisol (World Reference Base for Soil Resources; IUSS Working Group WRB, 2014), with the discontinuous and sporadic permafrost being widely distributed due to the cold climate on the plateau (Cheng & Wu, 2007). The main body of permafrost formed during the late Pleistocene Last Glaciation Maximum (LGM) (26,500-19,000 years BP, Zhou, Guo, Qiu, Cheng, & Li, 2000), but experienced extensive downward degradation after the warming period during the Megathermal in Holocene (8,500-4,000 years BP, Jin, Chang, & Wang, 2007). Subsequently, a new permafrost layer emerged during the Neoglaciation period (4,000-1,000 years BP, Jin et al., 2007). The current average active layer thickness is ~1.9 m (Zhao & Sheng, 2019) and increases at a rate of ~1.3 cm/year (Li et al., 2012).

Soil sampling and processing

Soil sampling was conducted across representative permafrost regions in late July and early August 2016 at 24 sites (Figure S1). Among these sampling sites, 10 sites were located along the Elashankou-Qingshuihe transect (eastern plateau), 3 sites were near the Qilian Mountains (northeastern plateau), and 11 sites were distributed along the Golmud-Amdo transect (the middle part of the plateau). Within each sampling site, one 10 m × 10 m plot was established, and three replicate cores were then drilled along a diagonal within the plot. These cores were drilled to a depth of 1.5-3.5 m which depended on the active layer thickness, with a borehole drilling machine (Liu et al., 2019). Based on these cores, we obtained soil samples from the active layer and the permafrost. Soil samples in the active layer were collected at the depth of 0-10 cm, since 90% of plant roots were concentrated in the top 30 cm soil across the study area (Yang, Fang, Ji, & Han, 2009). Correspondingly, the uppermost permafrost samples (50 cm thickness) were collected at ~25 cm below the thawfront during the sampling time (Figure S3). All soil samples were kept frozen during transportation and stored at -20 °C in the laboratory (Liu et al., 2019). Three days before the analyses, soil samples from the active layer were uniformly mixed after removing roots

and gravels quickly, and then temporarily kept at 4 °C. Meanwhile, permafrost samples were first broken into small pieces and then homogenized in a low-temperature environment.

Soil available N content and N transformation rates analyses

To compare soil N status of the permafrost and the active layer, we determined the soil initial available N content (NH_4^+, NO_3^- and DON content) and N transformation rates (net/gross N transformation rates) in these two soil layers. Specifically, fresh soils with the initial moisture content in the active layer and permafrost were extracted with 2 mol/L KCl, and then the content of NH_4^+ and NO_3^- as well as total dissolved N (TDN) were quantified with a flow injection analyzer (Autoanalyzer 3 SEAL, Bran and Luebbe, Norderstedt, Germany; the limit of detection is 0.003 mg N/L for NH_4^+ and 0.006 mg N/L for NO_3^-) and a C/N analyzer (multi-N/C 3100, Analytik Jena AG, Jena, Germany; the limit of detection is 0.05 mg N/L). The DON content was obtained by subtracting the DIN (NH_4^+ plus NO_3^-) content from the TDN content. Notably, the soil available N content was expressed as mg N per kg dry soil and g N per m^2 dry soil.

To simulate the natural drainage following permafrost thaw (Elberling et al., 2013), we conducted a drainage procedure on the permafrost samples before the incubation experiment. All the permafrost samples used for the laboratory incubation were drained freely at 5 °C for 48 hours using a sand bath (Elberling et al., 2013). However, drainage water was only collected from 10 of the 24 sampling sites, with the content of NH_4^+, NO_3^- and DON being with the range of 0.8-19.1, 0.01-0.15 and 0.1-1.3 mg N/kg, respectively (Table S1). Notably, the drainage procedure was not performed on samples in the active layer because their soil moisture was lower than 100% water-holding capacity (Figure S4). After the drainage, permafrost samples were preincubated at 5 °C for 7 days, which could equilibrate the microbial community in the thawed permafrost and satisfy the assumption of relatively stable microbial activity for the subsequent measurements of soil N transformation rates (Mao et al., 2019). Accordingly, soil samples in the active layer were also preincubated at 5 °C for 7 days to prevent pulses in microbial activity induced by disturbances during sample preparations.

After preincubation, both the soil net and gross N transformation rates were determined following the protocol (Hart, Stark, Davidson, & Firestone, 1994). For net N transformation rates, see Supplementary Information Text S1 for detailed descriptions. For gross N transformation rates, four subsamples (15 g each on an oven-dry basis) from each soil sample were labeled with ^{15}N: two were added with 100 μL $(^{15}NH_4)_2SO_4$ solution (0.33 mmol/L, ^{15}N at 30 atom%), and two received 100 μL $K^{15}NO_3$ solution (0.33 mmol/L, ^{15}N at 30 atom%). Afterwards, one subsample in each ^{15}N-labeled part was extracted with 2 mol/L KCl (T_0), and the other subsample was extracted with the same method after incubation in the dark at 5 °C for 1 day (T_1). It should be noted that the 5 °C was chosen based on the in-situ soil temperature in both permafrost and the active layer. Specifically, this selected temperature located between the average annual temperature at the top of permafrost (-1.1 °C; Zhang et al., 2020) and the mean annual soil temperature in the active layer at 10 cm depth (8.4 °C; China Meteorological Data Service Center, http://data.cma.cn/en). It should also be noted that one day was the time period commonly adopted to measure gross N transformation rates (Dannenmann, Gasche, Ledebuhr, & Papen, 2006) because of the limited microbial remineralization of the added ^{15}N during such a short incubation time (about 1-1.6% of added ^{15}N; Davidson, Hart, Shanks, & Firestone, 1991). Subsequently, the soil extracts were used for determining the content of NH_4^+ and NO_3^- with the same approach described above and the corresponding ^{15}N abundance.

The ^{15}N abundance of NH_4^+ and NO_3^- were analyzed following the published protocol (Dannenmann et al., 2006). First, the NH_4^+ in extracts was converted to ammonia (NH_3) by adding magnesium oxide (MgO), and then absorbed by filter papers (acidified with 10 μL of 1 mol/L oxalic acid each) to measure the ^{15}N abundance of NH_4^+. Second, the extracts were continuously diffused for 48 hours with two additional acidified filters. This process was demonstrated to efficiently remove the remaining NH_4^+ in the extractions (Zhang, Wen, Zhang, & Cai, 2017). Third, to determine the ^{15}N abundance of NO_3^-, the NO_3^- in extracts was transformed into NH_4^+ after adding Devarda's alloy, and then absorbed by new acidified filters in the form of NH_3.

Afterwards, the filter papers containing N from steps one and three were used to determine ^{15}N abundance based on an isotope ratio mass spectrometer (IRMS 20-22, SerCon, Crewe, UK; the limit of detection is 0.036 atom% ^{15}N). With the combination of the content of NH_4^+ and NO_3^- and their ^{15}N abundance, we quantified the gross N transformation rates based on equations (1-2; Kirkham & Bartholomew, 1954):

$$m = \frac{M_0 - M_1}{t} \times \frac{\ln(H_0 M_1 / H_1 M_0)}{\ln(M_0 / M_1)}, c \neq m \quad (1)$$

$$c = \frac{M_0 - M_1}{t} \times \frac{\ln(H_0 / H_1)}{\ln(M_0 / M_1)}, \mathrm{c} \neq m \quad (2)$$

where m = the rate of N production (mg N kg^{-1} day^{-1}),

c = the rate of N consumption (mg N kg^{-1} day^{-1}),

M_0 or M_1 = the N content at T_0 or T_1 (mg N/kg),

H_0 or H_1 = the ^{15}N content at T_0 or T_1 (mg N/kg),

t = time (one day for this study).

For the $^{15}NH_4^+$-labeled part, m and c refer to the gross N mineralization and NH_4^+ consumption rate, with M and H involving the NH_4^+ content. For the $^{15}NO_3^-$-labeled part, m and c represent the gross nitrification and NO_3^- immobilization rate, with M and H concerning the NO_3^- content. The NH_4^+ immobilization rate was the difference between the NH_4^+ consumption rate and the gross nitrification rate, and the microbial immobilization rate was then obtained by adding up the rate of NH_4^+ immobilization and NO_3^- immobilization. Notably, the gross N transformation rates were expressed as mg N per kg dry soil per day and mg N per m^2 dry soil per day.

Soil PLFA, enzyme activity and qPCR analyses

Soil phospholipid fatty acid (PLFA), enzyme activity and quantitative polymerase chain reaction (qPCR) analyses were conducted to evaluate effects of microbial properties on soil N transformation rates. For the soil PLFA analyses, PLFAs were extracted following the descriptions from Bossio and Scow (1998), and analyzed using a gas chromatograph (Agilent 6890, Agilent Technologies, CA, USA) and a MIDI Sherlock Microbial Identification System (MIDI Inc.,

Newark, DE, USA), after calibrating with standard solutions of FAME 19:0 (Matreya Inc., State College, PA, USA). The PLFAs were quantified to bacterial PLFAs (i14:0, i15:0, a15:0, i16:0, 16:1ω7c, i17:0, a17:0, cy17:0, 18:1ω7c and cy19:0) and fungal PLFAs (18:2ω6,9c) (Chen et al., 2016), and then were used to calculate the fungal:bacterial ratio.

We measured the activities of two soil enzymes, β-1,4-*N*-acetylglucosaminidase (NAG) and leucine aminopeptidase (LAP), which were involved in soil N cycling. Specifically, the NAG and LAP activity analyses were conducted following the protocol provided by Saiya-Cork, Sinsabaugh and Zak (2002). Briefly, 2 g of fresh soil was mixed with 91 mL of 50 mmol/L acetate buffer, with the pH of the buffer being adjusted to that of the corresponding soil sample. Soil suspension (200 μL) and the artificial fluorogenic substrates (50 μL, 200 μmol/L) were then dispensed into 96-well microplates. Meanwhile, the corresponding standard curve for each soil sample was conducted by using 200 μL of soil suspension and 50 μL of standard (4-methylumbelliferone (MUB) for NAG, 7-amino-4-methylcoumarin (AMC) for LAP) at concentrations of 0, 0.5, 1, 5, 10, 15 and 20 μmol/L. The artificial fluorogenic substrate was 4-MUB-*N*-acetyl-β-D-glucosaminide for NAG and L-Leucine-7-amino-4-methylcoumarin for LAP. All the microplates were incubated at 5 °C in the dark for 12 hours. The fluorescence was then determined at certain wavelengths (365 nm for excitation and 450 nm for emission) using a fluorometric spectrometer (Beckman Coulter DTX 880, Indianapolis, IN, USA). The soil enzyme activity of each sample was obtained by comparing the measured fluorescence with the fluorescence of standard curve and expressed as nmol activity per gram dry soil per hour.

The abundances of *amoA* genes for soil ammonia-oxidizing archaea (AOA) and bacteria (AOB) were quantified to explore the effects of specific microorganisms on soil nitrification rate. Specifically, the DNA was extracted from about 0.25 g of soil with the Power Soil DNA Isolation Kit (MoBio Laboratories, Carlsbad, CA, USA) following the manufacturer's protocol. The quantity and quality of DNA were examined with a NanoDrop-2000 (Thermo Fisher Scientific, Madison, WI, USA). Afterwards, the *amoA* genes abundances for AOA and AOB were estimated

by qPCR analyses with a StepOne Plus real-time PCR system (Applied Biosystems, Foster, CA, USA). The 20 μL PCR reaction mixture included 10 μL of SYBR Premix Ex Taq (TaKaRa Biotech Inc., Dalian, China), 0.4 μL of forward and reverse primers, 0.4 μL of ROX Reference Dye (50 ×), 6.8 μL of DNA-free water and 2 μL of DNA template. The primer details and PCR settings are summarized in Table S2. The standard curves were established with a 10-fold diluted series of plasmids, with $R^2 > 0.99$. Finally, the gene copy numbers were obtained for each sample by comparing the threshold cycle values of soil samples to those of the standard curves, and presented in per gram dry soil (copies/g).

Soil physical and chemical analyses

Soil physiochemical properties were quantified to explore the influences of edaphic factors on soil N transformation rates. Soil moisture was measured by oven-drying fresh soil at 105 °C for 24 hours. Soil texture was quantified with a particle size analyzer (Malvern Masterizer 2000, Malvern, Worcestershire, UK) after removing soil organic matter by hydrogen peroxide and carbonate by hydrochloric acid, respectively. Soil pH was analyzed in a 1:2.5 soil-deionized water mixture with a pH electrode (PB-10, Sartorius, Gottingen, Germany). Soil total N content was analyzed by an elemental analyzer (Vario EL III, Elementar, Hanau, Germany).

Statistical analyses

All data were tested for normality and log-transformed when necessary, and analyzed with the following four steps. First, we used linear mixed-effects models to explore the differences in soil available N content (*i.e.*, NH_4^+, NO_3^-, DIN and DON content) and N transformation rates (*i.e.*, rates of net/gross N mineralization, net/gross nitrification and microbial immobilization) between the permafrost and the active layer. The soil layer was treated as a fixed effect, and both the sampling site and the core were included as random effects in the linear mixed-effects models.

Second, we used linear mixed-effects models to examine the single variable relationships of soil N transformation rates with biotic (*e.g.*, microbial biomass, microbial community structure, enzyme

activity and the abundances of ammonia-oxidizing microorganisms) and abiotic variables (*e.g.*, soil moisture, pH, texture, NH_4^+, DIN and DON content). The explanatory variables (biotic and abiotic variables) were treated as fixed factors, and the sampling site was considered as a random factor in the linear mixed-effects models.

Third, we conducted multivariable stepwise regression analyses to select the optimal explanatory variables for soil N transformation rates from the biotic and abiotic variables described above. The final explanatory variables were selected based on the Akaike's information criterion corrected for the small sample size (AICc; the smallest AICc represented the optimal model; Burnham & Anderson, 2002). To avoid the strong collinearity among explanatory variables, the correlation coefficients among explanatory variables remaining in the simplified model were less than the standard threshold of $|r| = 0.7$ (Dormann et al., 2013). Finally, based on the optimal explanatory variables obtained above, we conducted variance partitioning analyses to explore the relative importance of various variables in regulating soil N transformation rates. All the statistical analyses were performed in R software v3.4.1 (R Development Core Team, 2017) using the *lme4* package (Bates, Mäechler, Bolker, & Walker, 2014).

Results

Vertical patterns of soil available N content and N transformation rates

The linear mixed-effects models analyses indicated that soil available N content exhibited significant differences between the permafrost and active layer (Figure 1). Specifically, the soil DIN and DON content in the permafrost were lower (DIN: 16.7 ± 2.4 (mean ± SE) *vs.* 28.0 ± 2.5 mg N/kg, $F = 19.6$, $P < 0.01$; DON: 3.0 ± 0.4 *vs.* 21.2 ± 2.0 mg N/kg, $F = 117.3$, $P < 0.01$), accounting for about 59.7% and 14.4% of those in the active layer, respectively. Soil NH_4^+ dominated DIN in both the permafrost and active layer, with the proportion being about 97.6% and 94.7%, respectively. Likewise, soil N transformation rates also differed significantly between the permafrost and the active layer. To be specific, the gross rates of N mineralization, microbial immobilization and nitrification in the permafrost were lower than those in the active layer (gross

N mineralization: 0.5 ± 0.04 (mean ± SE) *vs.* 3.5 ± 0.16 mg N kg^{-1} day^{-1}, $F = 513.1$, $P < 0.01$; microbial immobilization: 0.3 ± 0.02 *vs.* 2.8 ± 0.14 mg N kg^{-1} day^{-1}, $F = 406.9$, $P < 0.01$; gross nitrification: 0.1 ± 0.004 *vs.* 0.6 ± 0.030 mg N kg^{-1} day^{-1}; $F = 448.8$, $P < 0.01$; Figure 2), with the respective proportion being about 15.6%, 10.7% and 9.2%. Similar to the gross rates, the net rates of N mineralization and nitrification in the permafrost were also lower than those in the active layer (net N mineralization: 0.1 ± 0.01 (mean ± SE) *vs.* 0.4 ± 0.04 mg N kg^{-1} day^{-1}, $F = 92.6$, $P < 0.01$; net nitrification: 0.02 ± 0.002 *vs.* 0.30 ± 0.029 mg N kg^{-1} day^{-1}, $F = 123.8$, $P < 0.01$; Figure 3). Notably, the soil N status (*i.e.*, soil available N content and N transformation rates) was also consistently lower in the permafrost than that in the active layer on a per m^2 dry soil basis ($P < 0.01$; Figure S5). Moreover, in both the active layer and the permafrost, soil net N mineralization rate was positively correlated with gross N mineralization rate while showed no significant relationship with microbial immobilization rate, and soil net nitrification rate had a positive association with gross nitrification rate (Figure S6).

Drivers of soil N transformation rates over a broad geographic scale

The linear mixed-effects models analyses revealed significant relationships between the soil N transformation rates (net/gross N transformation rates) and potential drivers (biotic and abiotic factors). Specifically, in the active layer, the gross N mineralization rate was positively associated with the soil moisture, DON content, total PLFAs, NAG activity and LAP activity, but negatively correlated with the pH, sand content and fungal:bacterial ratio (Figure 4a); the microbial immobilization rate was positively associated with soil moisture, DIN content and total PLFAs, but negatively correlated with pH, sand content and fungal:bacterial ratio (Figure 4b); the gross nitrification rate had positive correlations with soil moisture, NH_4^+ content and AOA and AOB abundances, but exhibited negative relationships with pH and sand content (Figure 4c). Likewise, significant relationships were also observed between the gross N transformation rates and most of abovementioned variables in the permafrost, but no significant associations were found between gross N transformation rates and sand content as well as between gross nitrification rate and AOB abundance (Figure 4). In addition, for soil N mineralization, the net rate had similar potential

drivers with gross rate, but the net rate in permafrost did not exhibit any significant relationships with soil moisture, sand content, DON content and fungal:bacterial ratio (Figure S7a). Unlike the gross nitrification rate, net nitrification rate in the active layer was only positively correlated with soil moisture and NH_4^+ content, but negatively associated with sand content. Net nitrification rate in the permafrost only had positive relationships with soil moisture and NH_4^+ content while exhibited negative association with pH (Figure S7b).

The combination of stepwise regression analyses and variance partitioning analyses showed that the soil N transformation rates in the active layer and permafrost were regulated by different factors. To be specific, the gross rates of N mineralization and microbial immobilization in the active layer were mainly controlled by soil moisture (Figure 5a-b), while those in the permafrost were largely regulated by microbial properties (total PLFAs and fungal:bacterial ratio; Figure 5d-e). However, unlike N mineralization and immobilization rates, soil gross nitrification rates in both the active layer and permafrost were primarily influenced by NH_4^+ content (Figure 5c, f). It should be noted that the dominant drivers for the net N transformation rates were similar to those observed for the gross N transformation rates (Figure S8).

Discussion

To our knowledge, this study is the first attempt to reveal large-scale patterns and drivers of the available N pools and transformation rates in permafrost on the Tibetan Plateau (Figure 6). We observed consistent lower DIN (NH_4^+, NO_3^-) and DON content, as well as net/gross N transformation rates in the permafrost than those in the active layer. We also found that gross rates of N mineralization and microbial immobilization in the permafrost and active layer were regulated by different factors, with microbial properties (microbial biomass and fungal:bacterial ratio) dominating in the permafrost while soil moisture playing the most important role in the active layer. In contrast, gross nitrification rate was mainly modulated by soil NH_4^+ content in both the permafrost and active layer. Below, we discussed these findings by comparing the vertical patterns observed in this study with those reported in the Arctic region, and by comparing the

dominant drivers of soil N transformation rates between the permafrost and the active layer.

Contrasting vertical patterns of soil N content/transformation rates between Tibetan and Arctic permafrost region

Our results showed that soil available N content, including DIN and DON content, frozen in the Tibetan alpine permafrost was significantly lower than that in the active layer on both a per kg dry soil basis and a per m^2 dry soil basis (Figure 1, S5). This finding was different from the prevailing view that permafrost usually exhibited higher DIN and DON content than the active layer across the Arctic permafrost region (Beermann et al., 2017; Keuper et al., 2012; Salmon et al., 2018). It had been commonly recognized that permafrost microorganisms could survive at subzero temperature (Jansson & Taş, 2014; Mykytczuk et al., 2013) because of the unfrozen water in this deep sediment (Mader, Pettitt, Wadham, Wolff, & Parkes, 2006). The continuous microbial activity has been suggested as an important mechanism responsible for the available N pool in permafrost (Beermann et al., 2017). Based on these basic understandings, the contrasting patterns observed between the Tibetan and Arctic permafrost region could be associated with the different level of unfrozen water content in the permafrost. To test this possibility, we estimated the potential differences in permafrost unfrozen water content between these two regions by comparing the soil specific surface area (SSA), which played an important role in regulating the interaction of water molecules with the soil particles (Sepaskhah, Tabarzad, & Fooladmand, 2010). Specifically, based on the empirical model by Sepaskhah et al. (2010), we calculated the soil SSA of the permafrost using soil texture data in our study and also in a representative study from the Arctic region (Beermann et al., 2017), and found higher soil SSA in the Arctic permafrost (62.7 ± 11.2 (mean ± SE) *vs.* 27.5 ± 3.7 m^2/g; Figure S9). The larger soil SSA might lead to higher unfrozen water content in the Arctic permafrost (Anderson & Tice, 1972; Woo, 2012), which could provide favorable conditions for maintaining stronger microbial activity (Jansson & Taş, 2014) and facilitating available N production (Beermann et al., 2017). Given that permafrost might have lower soil available N consumption (*e.g.*, plant N uptake) than the active layer (Iversen et al., 2015), the promoted production of permafrost available N could accelerate its accumulation over

the long-term, thus leading to higher available N content in the permafrost than those in the active layer across the Arctic region. In contrast to the Arctic region, the markedly lower soil SSA in the Tibetan alpine permafrost could cause lower unfrozen water content (Anderson & Tice, 1972; Woo, 2012), which could then constrain microbial activity and subsequent available N production and accumulation in the permafrost. Consequently, the limited accumulation of permafrost available N could contribute to the lower available N content in the permafrost than that in the corresponding active layer across the Tibetan alpine permafrost region. Besides the microbial activity, the contrasting vertical patterns of available N content observed between the Tibetan and Arctic permafrost region could also be associated with the different proportions of total N content in the permafrost. In support of this point, evidences showed that soil total N content in the Arctic permafrost accounted for 78.2-189.8% of that in the corresponding active layer (Beermann et al., 2017; Keuper et al., 2012; Salmon et al., 2018), while this proportion was only 29.6% across the Tibetan alpine permafrost region (Figure S10a). Considering that soil total N pool was the source of substrate for available N production, the lower proportion of soil total N content in the permafrost relative to that in the active layer could thus lead to the lower vertical proportion of available N content across the Tibetan alpine permafrost region.

Our results also indicated that the Tibetan alpine permafrost had lower net N mineralization rate than the corresponding active layer on both a per kg dry soil basis and a per m^2 dry soil basis (Figure 3, S5), which was different from previous studies performed in the Arctic region (Keuper et al., 2012). The difference in the vertical patterns of net N mineralization rate could be associated with the different patterns of substrate supply and microbial activity observed in these two permafrost regions. Regarding the substrate supply, a previous study reported that the DON content in the permafrost was two times higher than that from the active layer in the Arctic region (Keuper et al., 2012), while the corresponding percentage was only 14.2% on the Tibetan Plateau (Figure S10b). Because DON is the substrate for microbial N mineralization (Kou et al., 2018), the distinct difference in DON content between the two soil layers might result in contrasting vertical patterns of net N mineralization rate between the two permafrost regions. Regarding the microbial

activity, it had been reported that the LAP activity in the permafrost was 1.9 times higher than that in the active layer in the Arctic region (Keuper et al., 2012), while the corresponding proportion was only about 10.2% across the Tibetan alpine permafrost region (Figure S10g). Given that soil extracellular enzymes were involved in catalyzing high-weight N compounds into small molecular compounds (*e.g.*, peptides and amino acids; Burns et al., 2013), the contrasting vertical patterns of LAP activity between the two soil layers could also lead to the opposite vertical trends in net N mineralization rate between the Tibetan and Arctic permafrost region.

Dominant drivers of soil gross N transformation rates in the permafrost and active layer

Our results revealed that soil moisture determined gross rates of N mineralization and microbial immobilization in the active layer (Figure 5). The determinant role of soil moisture in our study, together with previous findings in other drylands (Wang et al., 2016), jointly demonstrated the vital role of soil moisture in governing soil N cycle across arid ecosystems. The positive associations of soil gross N mineralization and microbial immobilization rates with soil moisture could be attributed to the following two aspects. On the one hand, elevated soil water availability could promote the accumulation of substrate for microorganisms (Delgado-Baquerizo et al., 2013). As the original source of substrate for microbial N mineralization and immobilization, soil total N is mainly derived from plant input (Yang, Ma, Mohammat, & Fang, 2007). It has been demonstrated that increased water availability can facilitate vegetation growth and organic matter input into the soils (Reid, Ogden, & Thoms, 2011; Yang et al., 2009), thereby promoting the subsequent accumulation of substrate for soil N transformation processes. In support of this argument, we observed positive relationships of soil total N, NH_4^+, NO_3^- and DON content with soil moisture across our sampling sites (Figure S11a-d). On the other hand, elevated soil water availability could also directly and indirectly enhance the microbial abundance and activity (Maestre et al., 2015). As the major control on substrate diffusion in arid soils, increased soil moisture could strongly reduce the diffusion limitation and elevate the amount of microbially accessible soluble substrate (Davidson, Samanta, Caramori, & Savage, 2012), further directly contributing to the stronger microbial activity (Hernández & Hobbie, 2010). In view of the

afore-mentioned role of soil moisture in accelerating the accumulation of soil organic matter, the increase in soil moisture could therefore elevate substrate availability for microbial communities (Maestre et al., 2015), thus indirectly improving microbial biomass and activity (Ding et al., 2016). Consistent with these deductions, positive associations of microbial abundance and enzyme activity with soil moisture were observed in our study region (Figure S11e-h). Collectively, soil moisture could govern the soil N mineralization/microbial immobilization rates through its effects on soil substrate supply and microbial abundance and activity.

Unlike its vital role in the active layer, the significance of soil moisture vanished in the permafrost, where microbial properties became the most important drivers of gross N mineralization and microbial immobilization rates (Figure 5). It is commonly recognized that microorganisms in the permafrost show lower abundance than those in the active layer due to the consistent low-temperature and -nutrient conditions (Jansson & Taş, 2014; Waldrop et al., 2010). Indeed, in our study, the total microbial biomass, bacterial biomass and fungal biomass were 91.3%, 93.9% and 95.3% lower in the permafrost than those in the active layer across our study sites, respectively (Figure S10c-e), suggesting that the low microbial abundance was the key constraint on soil N transformation rates after permafrost thaw. The dominant role of microbial biomass might be due to the fact that microorganisms are the direct participants in ecosystem N cycle and thus exert positive roles in soil N transformation processes (Booth, Stark, & Rastetter, 2005). Moreover, microbial biomass had a positive association with extracellular enzymes, which were involved in substrate production for soil N mineralization process (Schimel & Bennett, 2004; Li et al., 2019). In addition, the microbial necromass, associated with microbial biomass and produced by rapid microbial turnover, was reported to have positive effects on soil N mineralization and subsequent immobilization rates (Bonde, Schnürer, & Rosswall, 1988; Mikha, Rice, & Milliken, 2005). In addition to microbial biomass, the fungal:bacterial ratio was also an important driver of N mineralization and microbial immobilization rates in the permafrost. The negative impact of fungal:bacterial ratio on these two N processes could be partly attributed to the different population size of bacteria and fungi in soils (Strickland & Rousk, 2010). In the Tibetan alpine

permafrost, bacteria had much higher abundance than fungi, which might contribute to the greater role of bacteria in N mineralization and immobilization processes than that of fungi (Boyle, Yarwood, Bottomley, & Myrold, 2008) and thus lead to the negative effect of fungal:bacterial ratio on these processes. Additionally, it has also been reported that metabolic activity and N-demand are significantly higher in bacteria than in fungi (Kooijman, Bloem, van Dalen, & Kalbitz, 2016), thereby resulting in the negative association of N mineralization and microbial immobilization rates with fungal:bacterial ratio. Besides the microbial properties, both the gross N mineralization and microbial immobilization rates were also negatively associated with the permafrost sampling depth (Figure S12), reflecting vertical variations in these two rates. Nevertheless, these vertical variations should still be originally driven by environmental, substrate and microbial properties, *e.g.*, soil pH, DON content and microbial biomass.

Our results also illustrated that soil NH_4^+ content was the dominant driver of nitrification rate in both the permafrost and the active layer (Figure 5). Before discussing its potential mechanisms, we would like to mention that the nitrification process across the study area mainly referred to the autotrophic nitrification because of the limited heterotrophic nitrification in the study region (Kou et al., 2018). It is generally accepted that autotrophic nitrification is the biological oxidation of NH_3 to nitrite then to nitrate, and that the first process, NH_3 oxidation, is the rate-limiting step (Levy-Booth, Prescott, & Grayston, 2014). NH_3, which is mainly derived from NH_4^+ in soils, is thus the substrate for NH_3 oxidation, and AOA and AOB are the nitrifiers to drive NH_3 oxidation (Ouyang, Norton, & Stark, 2017). Nevertheless, the soil NH_4^+ is not only the source of substrate for autotrophic nitrification, but also is the direct substrate for NH_4^+ immobilization. More importantly, compared to autotrophic nitrification, NH_4^+ immobilization is more competitive for soil NH_4^+ since a greater number of microbes that participate in immobilization (Booth et al., 2005). The increase in soil NH_4^+ could alleviate the competition for substrate between the microbes participated in immobilization and nitrifiers, and might thus accelerate the nitrification process (Mao et al., 2019). In addition to the soil NH_4^+ content, the AOA abundance also regulated the nitrification process across the study area (Figure 5). This pattern might reflect the fact that

AOA is more efficient in utilizing NH_3 than AOB when the NH_3 content is low (Verhamme, Prosser, & Nicol, 2011).

In summary, based on the large-scale field investigation and the laboratory incubation experiment, combined with a ^{15}N pool dilution technique, enzyme activity and functional gene analyses, this study revealed the permafrost N status and its key drivers on the Tibetan Plateau. Our results showed that, unlike the Arctic, the Tibetan alpine permafrost contained lower available N content and net N mineralization rate than the active layer, suggesting that the permafrost N status was region-specific. In other words, the patterns observed in the Arctic (Finger et al., 2016; Salmon et al., 2016) could not be simply extended to the Tibetan alpine permafrost region. Moreover, the fate of the released N upon permafrost thaw might also be different in the two permafrost regions. Particularly, given that the Tibetan alpine permafrost region has a deeper active layer thickness (~1.9 m; Zhao & Sheng, 2019), but more than 90% of the plant roots are distributed within the top 30 cm depth (Yang et al., 2009), the impact of permafrost N release on vegetation growth may thus be limited across this permafrost region. Nevertheless, considering that the Tibetan Plateau was known as the 'Water Tower of Asia' (Immerzeel et al., 2010), the available N released from thawing permafrost could be leached into the surrounding aquatic ecosystems, which might alter the structure and function of these ecosystems (Harms & Jones, 2012; Wickland et al., 2018). In addition, the available N released upon permafrost thaw could be emitted into the atmosphere as the form of N_2O, intensifying the noncarbon feedback to climate warming (Voigt et al., 2017; Yang et al., 2018). Our results also revealed that the dominant drivers of N mineralization/immobilization processes differed between the permafrost and the active layer. The depth-dependent drivers of soil N transformation rates should be integrated into process-based biogeochemistry models when resolving carbon and N cycles with soil depth. More importantly, our results illustrated that microbial properties played a crucial role in mediating soil N transformation processes in the permafrost, highlighting that the incorporation of microbial properties into model structure was essential to better evaluate the permafrost biogeochemical cycle and its feedbacks to climate warming.

While our study evaluates the permafrost N status sufficiently, some uncertainties still exist. First, soil N transformation processes were only determined under aerobic conditions by simulating the natural drainage following permafrost thaw in uplands (Elberling et al., 2013). Nevertheless, the poorly drained soil conditions with anoxia also occur in some lowland areas although the Tibetan permafrost is majorly distributed in upland areas with good drainage (Chen et al., 2016). Future studies should consider both aerobic and anaerobic conditions to better understand the hydrological effects on soil N transformation processes. Second, soil N transformation rates were only measured once after 7 days of pre-incubation. Nevertheless, the rapid shifts in microbial community composition and metabolic rates have been identified during and following permafrost thaw (Mackelprang et al., 2011). One single measurement is thus insufficient to fully characterize the microbial dynamics. Extending studies with multiple determination of soil N transformation rates could further improve our understanding on the dynamics of microbial processes after permafrost thaw.

Acknowledgments

We thank four anonymous reviewers who have provided constructive comments to improve this manuscript, and appreciate Dr. Yongliang Chen for his help during the field investigation. We also acknowledge the financial support from the National Natural Science Foundation of China (31825006, 31988102, and 91837312), the Second Tibetan Plateau Scientific Expedition and Research (STEP) program (2019QZKK0106 and 2019QZKK0302), and Key Research Program of Frontier Sciences, Chinese Academy of Sciences (QYZDB-SSW-SMC049).

Conflict of Interest

The authors declare that they have no conflict of interest.

Data Availability Statement

All related data are available on request from the corresponding author (Dr. Yuanhe Yang).

ORCID

Yuanhe Yang: https://orcid.org/0000-0002-5399-4606

References

Aalto, J., Karjalainen, O., Hjort, J., & Luoto, M. (2018). Statistical forecasting of current and future circum-Arctic ground temperatures and active layer thickness. *Geophysical Research Letters, 45*(10), 4889-4898. https://doi.org/10.1029/2018GL078007

Anderson, D. M., & Tice, A. R. (1972). Predicting unfrozen water contents in frozen soils from surface area measurements. *Highway Research Record,* 393, 12-18.

Bates, D., Mäechler, M., Bolker, B., & Walker, S. (2015). Fitting linear mixed-effects models using lme4. *Journal of Statistical Software, 67*(1), 1-48. https://doi.org/10.18637/jss.v067.i01

Beermann, F., Langer, M., Wetterich, S., Strauss, J., Boike, J., Fiencke, C., . . . Kutzbach, L. (2017). Permafrost thaw and liberation of inorganic nitrogen in eastern Siberia. *Permafrost and Periglacial Processes, 28*(4), 605-618. https://doi.org/10.1002/ppp.1958

Biskaborn, B. K., Smith, S. L., Noetzli, J., Matthes, H., Vieira, G., Streletskiy, D. A., . . . Lantuit, H. (2019). Permafrost is warming at a global scale. *Nature Communications, 10*, 264. https://doi.org/10.1038/s41467-018-08240-4

Bonde, T. A., Schnürer, J., & Rosswall, T. (1988). Microbial biomass as a fraction of potentially mineralizable nitrogen in soils from long-term field experiments. *Soil Biology & Biochemistry, 20*, 447-452. https://doi.org/10.1016/0038-0717(88)90056-9

Booth, M. S., Stark, J. M., & Rastetter, E. (2005). Controls on nitrogen cycling in terrestrial ecosystems: a synthetic analysis of literature data. *Ecological Monographs, 75*(2), 139-157. https://doi.org/10.1890/04-0988

Bossio, D. A., & Scow, K. M. (1998). Impacts of carbon and flooding on soil microbial communities: phospholipid fatty acid profiles and substrate utilization patterns. *Microbial Ecology, 35*, 265-278. https://doi.org/10.1007/s002489900082

Boyle, S. A., Yarwood, R. R., Bottomley, P. J., & Myrold, D. D. (2008). Bacterial and fungal contributions to soil nitrogen cycling under Douglas fir and red alder at two sites in Oregon. *Soil Biology & Biochemistry, 40*, 443-451. https://doi.org/10.1016/j.soilbio.2007.09.007

Burnham, K. P., & Anderson, D. R. (2002). *Model Selection and Multimodel Inference*. New York, NY: Springer.

Burns, R. G., DeForest, J. L., Marxsen, J., Sinsabaugh, R. L., Stromberger, M. E., Wallenstein, M. D., . . . Zoppini, A. (2013). Soil enzymes in a changing environment: current knowledge and future directions. *Soil Biology & Biochemistry*, *58*, 216-234. http://doi.org/10.1016/j.soilbio.2012.11.009

Chadburn, S. E., Burke, E. J., Cox, P. M., Friedlingstein, P., Hugelius, G., & Westermann, S. (2017). An observation-based constraint on permafrost loss as a function of global warming. *Nature Climate Change, 7*, 340-345. https://doi.org/10.1038/nclimate3262

Chen, L., Liang, J., Qin, S., Li, L., Kai, F., Xu, Y., . . . Yang, Y. (2016). Determinants of carbon release from the active layer and permafrost deposits on the Tibetan Plateau. *Nature Communications, 7*, 13046. https://doi.org/10.1038/ncomms13046

Chen, L., Liu, L., Mao, C., Qin, S., Wang, J., Liu, F., . . . Yang, Y. (2018). Nitrogen availability regulates topsoil carbon dynamics after permafrost thaw by altering microbial metabolic efficiency. *Nature Communications, 9*, 3951. https://doi.org/10.1038/s41467-018-06232-y

Cheng, G., & Wu, T. (2007). Responses of permafrost to climate change and their environmental significance, Qinghai-Tibet Plateau. *Journal of Geophysical Research: Earth Surface, 112*, F02S03. https://doi.org/10.1029/2006JF000631

Dannenmann, M., Gasche, R., Ledebuhr, A., & Papen, H. (2006). Effects of forest management on soil N cycling in beech forests stocking on calcareous soils. *Plant and Soil, 287*, 279-300. https://doi.org/10.1007/s11104-006-9077-4

Davidson, E. A., Hart, S. C., Shanks, C. A., & Firestone, M. K. (1991). Measuring gross nitrogen mineralization, immobilization, and nitrification by ^{15}N isotopic pool dilution in intact soil cores. *Journal of Soil Science, 42*, 335-349. https://doi.org/10.1111/j.1365-2389.1991.tb00413.x

Davidson, E. A., Samanta, S., Caramori, S. S., & Savage, K. (2012). The Dual Arrhenius and Michaelis-Menten kinetics model for decomposition of soil organic matter at hourly to seasonal time scales. *Global Change Biology, 18*(1), 371-384. https://doi.org/10.1111/j.1365-2486.2011.02546.x

Delgado-Baquerizo, M., Maestre, F. T., Gallardo, A., Bowker, M. A., Wallenstein, M. D., Quero, J. L., . . . Zaady, E. (2013). Decoupling of soil nutrient cycles as a function of aridity in global drylands. *Nature, 502*, 672-676. https://doi.org/10.1038/nature12670

Ding, J., Chen, L., Zhang, B., Liu, L., Yang, G., Fang, K., . . . Yang, Y. (2016). Linking temperature sensitivity of soil CO_2 release to substrate, environmental, and microbial properties across alpine ecosystems. *Global Biogeochemical Cycles, 30*(9), 1310-1323. https://doi.org/10.1002/2015GB005333

Dormann, C. F., Elith, J., Bacher, S., Buchmann, C., Carl, G., Carré, G., . . . Lautenbach, S. (2013). Collinearity: a review of methods to deal with it and a simulation study evaluating their performance. *Ecography, 36*(1), 27-46. https:// doi.org/10.1111/j.1600-0587.2012.07348.x

Elberling, B., Michelsen, A., Schädel, C., Schuur, E. A. G., Christiansen, H. H., Berg, L., . . . Sigsgaard, C. (2013). Long-term CO_2 production following permafrost thaw. *Nature Climate Change, 3*, 890-894. https://doi.org/10.1038/nclimate1955

Finger, R. A., Turetsky, M. R., Kielland, K., Ruess, R. W., Mack, M. C., & Euskirchen, E. S. (2016). Effects of permafrost thaw on nitrogen availability and plant-soil interactions in a boreal Alaskan lowland. *Journal of Ecology, 104*(6), 1542-1554. https://doi.org/10.1111/1365-2745.12639

Harden, J. W., Koven, C. D., Ping, C.-L., Hugelius, G., McGuire, A. D., Camill, P., . . . Grosse, G. (2012). Field information links permafrost carbon to physical vulnerabilities of thawing. *Geophysical Research Letters, 39*, L15704. https://doi.org/10.1029/2012GL051958

Harms, T. K., & Jones Jr, J. B. (2012). Thaw depth determines reaction and transport of inorganic nitrogen in valley bottom permafrost soils: nitrogen cycling in permafrost soils. *Global Change Biology, 18*(9), 2958-2968. https://doi.org/10.1111/j.1365-2486.2012.02731.x

Hart, S. C., Stark, J. M., Davidson, E. A., & Firestone, M. K. (1994). *Nitrogen mineralization,*

immobilization, and nitrification. Madison, WI: Soil Science Society of America.

Hernández, D. L., & Hobbie, S. E. (2010). The effects of substrate composition, quantity, and diversity on microbial activity. *Plant and Soil*, *335*, 397-411. https://doi.org/10.1007/s11104-010-0428-9

Hu, G., Zhao, L., Li, R., Wu, X., Wu, T., Xie, C., . . . Su, Y. (2019). Variations in soil temperature from 1980 to 2015 in permafrost regions on the Qinghai-Tibetan Plateau based on observed and reanalysis products. *Geoderma, 337*, 893-905. https://doi.org/10.1016/j.geoderma.2018.10.044

Immerzeel, W. W., Van Beek, L. P. H., & Bierkens, M. F. P. (2010). Climate change will affect the Asian water towers. *Science, 328*(5984), 1382-1385. https://doi.org/10.1126/science.1183188

IUSS Working Group WRB (2014). *World Reference Base for Soil Rescources 2014*. International soil classification system for naming soils and creating legends for soil maps. World Soil Resources Reports No. 106. FAO, Rome.

Iversen, C. M., Sloan, V. L., Sullivan, P. F., Euskirchen, E. S., Mcguire, A. D., Norby, R. J., . . . Wullschleger, S. D. (2015). The unseen iceberg: plant roots in arctic tundra. *New Phytologist*, *205*(1), 34-58. https://doi.org/10.1111/nph.13003

Jansson, J. K., & Taş, N. (2014). The microbial ecology of permafrost. *Nature Reviews Microbiology, 12*, 414-425. https://doi.org/10.1038/nrmicro3262

Jin, H., Chang, X., & Wang, S. (2007). Evolution of permafrost on the Qinghai-Xizang (Tibet) Plateau since the end of the late Pleistocene. *Journal of Geophysical Research: Earth Surface, 112*, F02S09. https://doi.org/10.1029/2006JF000521

Keuper, F., Dorrepaal, E., van Bodegom, P. M., Van, L. R., Venhuizen, G., Van, H. J., & Aerts, R. (2017). Experimentally increased nutrient availability at the permafrost thaw front selectively enhances biomass production of deep-rooting subarctic peatland species. *Global Change Biology, 23*(10), 4257-4266. https://doi.org/10.1111/gcb.13804

Keuper, F., van Bodegom, P. M., Dorrepaal, E., Weedon, J. T., van Hal, J., van Logtestijn, R. S. P., & Aerts, R. (2012). A frozen feast: thawing permafrost increases plant-available nitrogen

in subarctic peatlands. *Global Change Biology, 18*(6), 1998-2007. http://doi.org/10.1111/j.1365-2486.2012.02663.x

Kirkham, D., & Bartholomew, W. V. (1954). Equations for following nutrient transformations in soil, utilizing tracer data. *Soil Science Society of America Journal, 18*(1), 33-34. http://doi.org/10.2136/sssaj1954.03615995001800010009x

Kooijman, A., Bloem, J., van Dalen, B., & Kalbitz, K. (2016). Differences in activity and N demand between bacteria and fungi in a microcosm incubation experiment with selective inhibition. *Applied Soil Ecology, 99*, 29-39. https://doi.org/10.1016/j.apsoil.2015.11.011

Kou, D., Ding, J., Li, F., Wei, N., Fang, K., Yang, G., . . . Chen, Y. (2019). Spatially-explicit estimate of soil nitrogen stock and its implication for land model across Tibetan alpine permafrost region. *Science of the Total Environment, 650*, 1795-1804. https://doi.org/10.1016/j.scitotenv.2018.09.252

Kou, D., Peng, Y., Wang, G., Ding, J., Chen, Y., Yang, G., . . . Müller, C. (2018). Diverse responses of belowground internal nitrogen cycling to increasing aridity. *Soil Biology & Biochemistry, 116*, 189-192. https://doi.org/10.1016/j.soilbio.2017.10.010

Levy-Booth, D. J., Prescott, C. E., & Grayston, S. J. (2014). Microbial functional genes involved in nitrogen fixation, nitrification and denitrification in forest ecosystems. *Soil Biology & Biochemistry*, *75*, 11-25. https://doi.org/10.1016/j.soilbio.2014.03.021

Li, R., Zhao, L., Ding, Y., Wu, T., Xiao, Y., Du, E., . . . Qiao, Y. (2012). Temporal and spatial variations of the active layer along the Qinghai-Tibet Highway in a permafrost region. *Chinese Science Bulletin, 57*, 4609-4616. https://doi.org/10.1007/s11434-012-5323-8

Li, Z., Tian, D., Wang, B., Wang, J., Wang, S., Chen, H. Y., . . . Niu, S. (2019). Microbes drive global soil nitrogen mineralization and availability. *Global Change Biology, 25*(3), 1078-1088. https://doi.org/10.1111/gcb.14557

Liu, F., Kou, D., Abbott, B. W., Mao, C., Chen, Y., Chen, L., & Yang, Y. (2019). Disentangling the effects of climate, vegetation, soil and related substrate properties on the biodegradability of permafrost-derived dissolved organic carbon. *Journal of Geophysical Research: Biogeosciences, 124*(11), 3377-3389. https://doi.org/10.1029/2018JG004944

Mader, H. M., Pettitt, M. E., Wadham, J. L., Wolff, E. W., & Parkes, R. J. (2006). Subsurface ice as a microbial habitat. *Geology, 34*(3), 169-172. https://doi.org/10.1130/G22096.1

Mackelprang, R., Waldrop, M. P., DeAngelis, K. M., David, M. M., Chavarria, K. L., Blazewicz, S. J., . . . Jansson, J. K. (2011). Metagenomic analysis of a permafrost microbial community reveals a rapid response to thaw. *Nature, 480*, 368-371. https://doi.org/10.1038/nature10576

Maestre, F. T., Delgado-Baquerizo, M., Jeffries, T. C., Eldridge, D. J., Ochoa, V., Gozalo, B., . . . Ulrich, W. (2015). Increasing aridity reduces soil microbial diversity and abundance in global drylands. *Proceedings of the National Academy of Sciences of the United States of America, 112*(51), 15684-15689. https://doi.org/10.1073/pnas.1516684112

Mao, C., Kou, D., Wang, G., Peng, Y., Yang, G., Liu, F., . . . Yang, Y. (2019). Trajectory of topsoil nitrogen transformations along a thermo-erosion gully on the Tibetan Plateau. *Journal of Geophysical Research: Biogeosciences, 124*(5), 1342-1354. https://doi.org/10.1029/2018JG004805

Mikha, M. M., Rice, C. W., & Milliken, G. A. (2005). Carbon and nitrogen mineralization as affected by drying and wetting cycles. *Soil Biology & Biochemistry, 37*, 339-347. https://doi.org/10.1016/j.soilbio.2004.08.003

Mu, C., Zhang, T., Wu, Q., Cao, B., Zhang, X., Peng, X., . . . Cheng, G. (2015). Carbon and nitrogen properties of permafrost over the Eboling Mountain in the upper reach of Heihe River basin, northwestern China. *Arctic, Antarctic, and Alpine Research, 47*(2), 203-211. https://doi.org/10.1657/AAAR00C-13-095

Mykytczuk, N. C. S., Foote, S. J., Omelon, C. R., Southam, G., Greer, C. W., & Whyte, L. G. (2013). Bacterial growth at -15 °C; molecular insights from the permafrost bacterium *Planococcus halocryophilus* Or1. *The ISME Journal, 7*, 1211-1226. https://doi.org/10.1038/ismej.2013.8

Ouyang, Y., Norton, J. M., & Stark, J. M. (2017). Ammonium availability and temperature control contributions of ammonia oxidizing bacteria and archaea to nitrification in an agricultural soil. *Soil Biology & Biochemistry, 113*, 161-172. https://doi.org/10.1016/j.soilbio.2017.06.010

R Development Core Team (2017). *R: A Language and Environment for Statistical Computing*. Vienna, Austria: R Foundation for Statistical Computing.

Ran, Y., Li, X., & Cheng, G. (2018). Climate warming over the past half century has led to thermal degradation of permafrost on the Qinghai-Tibet Plateau. *The Cryosphere, 12*, 595-608. https://doi.org/10.5194/tc-12-595-2018

Reid, M. A., Ogden, R., & Thoms, M. C. (2011). The influence of flood frequency, geomorphic setting and grazing on plant communities and plant biomass on a large dryland floodplain. *Journal of Arid Environments, 75*(9), 815-826. https://doi.org/10.1016/j.jaridenv.2011.03.014

Saiya-Cork, K. R., Sinsabaugh, R. L., & Zak, D. R. (2002). The effects of long term nitrogen deposition on extracellular enzyme activity in an *Acer saccharum* forest soil. *Soil Biology & Biochemistry, 34*, 1309-1315. https://doi.org/10.1016/S0038-0717(02)00074-3

Salmon, V. G., Schädel, C., Bracho, R., Pegoraro, E., Celis, G., Mauritz, M., . . . Schuur, E. A. G. (2018). Adding depth to our understanding of nitrogen dynamics in permafrost soils. *Journal of Geophysical Research: Biogeosciences, 123*(8), 2497-2512. https://doi.org/10.1029/2018JG004518

Salmon, V. G., Soucy, P., Mauritz, M., Celis, G., Natali, S. M., Mack, M. C., & Schuur, E. A. G. (2016). Nitrogen availability increases in a tundra ecosystem during five years of experimental permafrost thaw. *Global Change Biology, 22*(5), 1927-1941. https://doi.org/10.1111/gcb.13204

Schimel, J. P., & Bennett, J. (2004). Nitrogen mineralization: challenges of a changing paradigm. *Ecology*, *85*(3), 591-602. https://doi.org/10.1890/03-8002

Sepaskhah, A. R., Tabarzad, A., & Fooladmand, H. R. (2010). Physical and empirical models for estimation of specific surface area of soils. *Archives of Agronomy and Soil Science, 56*(3), 325-335. https://doi.org/10.1080/03650340903099676

Strickland, M. S., & Rousk, J. (2010). Considering fungal:bacterial dominance in soils - methods, controls, and ecosystem implications. *Soil Biology & Biochemistry*, *42*, 1385-1395. https://doi.org/10.1016/j.soilbio.2010.05.007

Treat, C. C., Wollheim, W. M., Varner, R. K., Grandy, A. S., Talbot, J., & Frolking, S. (2014). Temperature and peat type control CO_2 and CH_4 production in Alaskan permafrost peats. *Global Change Biology, 20*(8), 2674-2686. https://doi.org/10.1111/gcb.12572

USDA (1999). *Soil Taxonomy: A Basic System of Soil Classification for Making and Interpreting Soil Surveys*. Agriculture Handbook No. 436, 2nd edn. US Department of Agriculture, Natural Resources Conservation Service, Washington, DC, USA.

Verhamme, D. T., Prosser, J. I., & Nicol, G. W. (2011). Ammonia concentration determines differential growth of ammonia-oxidising archaea and bacteria in soil microcosms. *The ISME Journal*, *5*, 1067-1071. https:// doi.org/10.1038/ismej.2010.191

Voigt, C., Marushchak, M. E., Lamprecht, R. E., Jackowicz-Korczyński, M., Lindgren, A., Mastepanov, M., . . . Martikainen, P. J. (2017). Increased nitrous oxide emissions from Arctic peatlands after permafrost thaw. *Proceedings of the National Academy of Sciences of the United States of America, 114*(24), 6238-6243. https://doi.org/10.1073/pnas.1702902114

Vonk, J. E., Tank, S. E., Bowden, W. B., Laurion, I., Vincent, W. F., Alekseychik, P., . . . Wickland, K. P. (2015). Reviews and syntheses: effects of permafrost thaw on Arctic aquatic ecosystems. *Biogeosciences, 12*, 7129-7167. https://doi.org/10.5194/bg-12-7129-2015

Waldrop, M. P., Wickland, K. P., White, R., Iii, Berhe, A. A., Harden, J. W., & Romanovsky, V. E. (2010). Molecular investigations into a globally important carbon pool: permafrost-protected carbon in Alaskan soils. *Global Change Biology,* 16(9), 2543-2554. https://doi.org/10.1111/j.1365-2486.2009.02141.x

Wang, B., & French, H. (1995). Permafrost on the Tibet Plateau, China. *Quaternary Science Reviews, 14*(3), 255-274. https://doi.org/10.1016/0277-3791(95)00006-B

Wang, J., Wang, L., Feng, X., Hu, H., Cai, Z., Müller, C., & Zhang, J. (2016). Soil N transformations and its controlling factors in temperate grasslands in China: a study from ^{15}N tracing experiment to literature synthesis. *Journal of Geophysical Research: Biogeosciences, 121*(12), 2949-2959. https://doi.org/10.1002/2016JG003533

Wang, W., Ma, Y., Xu, J., Wang, H., Zhu, J., & Zhou, H. (2012). The uptake diversity of soil nitrogen nutrients by main plant species in Kobresia humilis alpine meadow on the Qinghai-Tibet Plateau. *Science China Earth Sciences, 55*, 1688-1695. https://doi.org/10.1007/s11430-012-4461-9

Wickland, K. P., Waldrop, M. P., Aiken, G. R., Koch, J. C., Jorgenson, M. T., & Striegl, R. G. (2018). Dissolved organic carbon and nitrogen release from boreal Holocene permafrost and seasonally frozen soils of Alaska. *Environmental Research Letters, 13*, 065011. https://doi.org/10.1088/1748-9326/aac4ad

Wild, B., Schnecker, J., Bárta, J., Čapek, P., Guggenberger, G., Hofhansl, F., . . . Richter, A. (2013). Nitrogen dynamics in Turbic Cryosols from Siberia and Greenland. *Soil Biology & Biochemistry, 67*, 85-93. https://doi.org/10.1016/j.soilbio.2013.08.004

Woo, M. (2012). *Permafrost Hydrology*. New York, NY: Springer.

Xu, X., Ouyang, H., Richter, A., Wanek, W., Cao, G., & Kuzyakov, Y. (2011). Spatio-temporal variations determine plant-microbe competition for inorganic nitrogen in an alpine meadow. *Journal of Ecology, 99*(2), 563-571. https://doi.org/10.1111/j.1365-2745.2010.01789.x

Yang, G., Peng, Y., Marushchak, M., Chen, Y., Wang, G., Li, F., . . . Yang, Y. (2018). Magnitude and pathways of increased nitrous oxide emissions from uplands following permafrost thaw. *Environmental Science & Technology, 52*(16), 9162-9169. https://doi.org/10.1021/acs.est.8b02271

Yang, M., Nelson, F. E., Shiklomanov, N. I., Guo, D., & Wan, G. (2010). Permafrost degradation and its environmental effects on the Tibetan Plateau: a review of recent research. *Earth-Science Reviews, 103*(1-2), 31-44. https://doi.org/10.1016/j.earscirev.2010.07.002

Yang, Y., Fang, J., Ji, C., & Han, W. (2009). Above- and belowground biomass allocation in Tibetan grasslands. *Journal of Vegetation Science, 20*(1), 177-184. https://doi.org/10.1111/j.1654-1103.2009.05566.x

Yang, Y., Ma, W., Mohammat, A., & Fang, J. (2007). Storage, patterns and controls of soil nitrogen in China. *Pedosphere, 17*(6), 776-785.

https://doi.org/10.1016/S1002-0160(07)60093-9

Zhang, J., Wang, J. T., Chen, W., Li, B., & Zhao, K. (1988). *Vegetation of Xizang (Tibet)*. Beijing: Science Press.

Zhang, P., Wen, T., Zhang, J., & Cai, Z. (2017). On improving the diffusion method for determination of $\delta^{15}N\text{-}NH_4^+$ and $\delta^{15}N\text{-}NO_3^-$ in soil extracts. *Acta Pedologica Sinica, 54*(4), 948-957. https://doi.org/10.11766/trxb201611250485

Zhang, T., Barry, R. G., Knowles, K., Heginbottom, J. A., & Brown, J. (1999). Statistics and characteristics of permafrost and ground-ice distribution in the Northern Hemisphere. *Polar Geography, 23*(2), 132-154. https://doi.org/10.1080/10889379909377670

Zhang, Z., Wu, Q., Jiang, G., Gao, S., Chen, J., & Liu, Y. (2020). Changes in the permafrost temperatures from 2003 to 2015 in the Qinghai-Tibet Plateau. *Cold Regions Science and Technology, 169*, 102904. https://doi.org/10.1016/j.coldregions.2019.102904

Zhao, L., & Sheng, Y. (2019). *Permafrost and its Changes on the Qinghai-Tibetan Plateau*. Beijing: Science Press.

Zhou, Y., Guo, D., Qiu, G., Cheng, G., & Li, S. (2000). *Geocryology in China*. Beijing: Science Press.

Figure Legends

Figure 1 Spatial variations of the differences in soil NH_4^+-N (a), NO_3^--N (b), dissolved inorganic N (DIN, c) and dissolved organic N (DON, d) content between the permafrost and the active layer across 24 sampling sites along the permafrost transect. ΔN content = N $content_{permafrost}$ - N $content_{active\ layer}$. The area of the bubble relates to the size of absolute value of the corresponding ΔN content. The orange and blue bubbles indicate positive and negative values, respectively. The embedded violin plots indicate the comparison of corresponding N content between the permafrost (PF) and active layer (AL). The whiskers represent the 5th and 95th quartiles, and the box ends illustrate the 25th and 75th quartiles (interquartile range). $^{**}P < 0.01$. See Table S3 for the corresponding standard error (SE) at each sampling site.

Figure 2 Spatial variations of the differences in soil gross rates of N mineralization (GNM, a), microbial immobilization (MIM, b) and nitrification (GN, c) between the permafrost and active layer across 24 sampling sites along the permafrost transect. Δrate = $rate_{permafrost}$ - $rate_{active\ layer}$. The area of the bubble relates to the size of the absolute value of corresponding Δrate. The blue bubbles indicate negative values. The embedded violin plots indicate the comparison of corresponding N transformation rates between the permafrost (PF) and active layer (AL). The whiskers represent the 5th and 95th quartiles, and the box ends illustrate the 25th and 75th quartiles (interquartile range). ** $P < 0.01$. See Table S4 for the corresponding standard error (SE) at each sampling site.

Figure 3 Spatial variations of the difference in soil net rates of N mineralization (NNM, a) and nitrification (NN, b) between the permafrost and active layer across 24 sampling sites along the permafrost transect. Δrate = $rate_{permafrost} - rate_{active\ layer}$. The area of the bubble relates to the size of the absolute value of corresponding Δrate. The orange and blue bubbles indicate positive and negative values, respectively. The embedded violin plots indicate the comparison of corresponding net N transformation rates between the permafrost (PF) and active layer (AL). The whiskers represent the 5th and 95th quartiles, and the box ends illustrate the 25th and 75th quartiles

(interquartile range). ** $P < 0.01$. See Table S4 for the corresponding standard error (SE) at each sampling site.

Figure 4 Proportions for the gross rates of N mineralization (a), microbial immobilization (b) and nitrification (c) explained by the biotic and abiotic variables in the active layer and the permafrost. The values of the radiuses of the grey circles are shown as the vertical scales. The lengths of the bars are proportional to the radiuses of the grey circles and represent the explained proportions. The orange and blue bars indicate positive and negative correlations between N transformation rates and the explanatory variables, respectively. DON, dissolved organic N; DIN, dissolved inorganic N; PLFAs, phospholipid fatty acids; F/B, the ratio of fungal to bacterial PLFAs; NAG, β-1,4-*N*-acetylglucosaminidase; LAP, leucine aminopeptidase; AOA, ammonia-oxidizing archaea; AOB, ammonia-oxidizing bacteria. * $P < 0.05$, ** $P < 0.01$.

Figure 5 Results of variation partitioning analyses for the gross rates of N mineralization (a, d), microbial immobilization (b, e) and nitrification (c, f) in the active layer and permafrost. PLFAs, phospholipid fatty acids; F/B, the ratio of fungal to bacterial FLFAs; AOA, ammonia-oxidizing archaea. X1 and X3 indicate the pure effect of each variable, and X2 suggests the joint effect of two variables.

Figure 6 Schematic representation of soil available N content and N transformation rates in the active layer and permafrost on the Tibetan Plateau. The area of the circle is proportional to the amount of available N, and the arrow width is proportional to the value of N transformation rate. The biotic and abiotic factors adjacent to arrows are the dominant drivers for the corresponding N transformation rates. The microbial properties referred to soil microbial biomass and the ratio of fungal to bacterial PLFAs, and the substrate referred to soil NH_4^+ content. Available N includes NH_4^+, NO_3^- and dissolved organic N (DON). PLFAs, phospholipid fatty acids. MBN, microbial nitrogen.

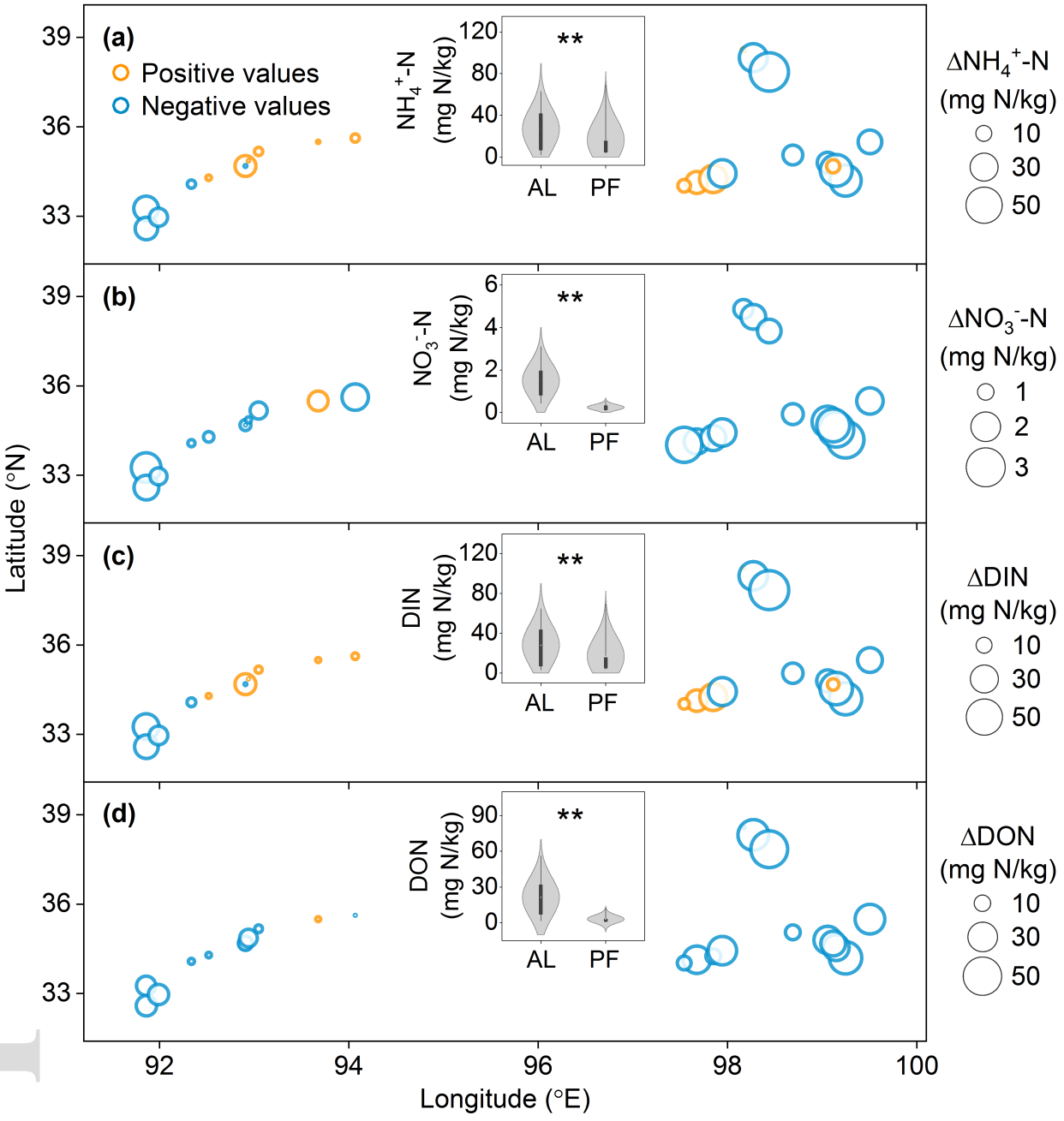

gcb_15205_f1.png

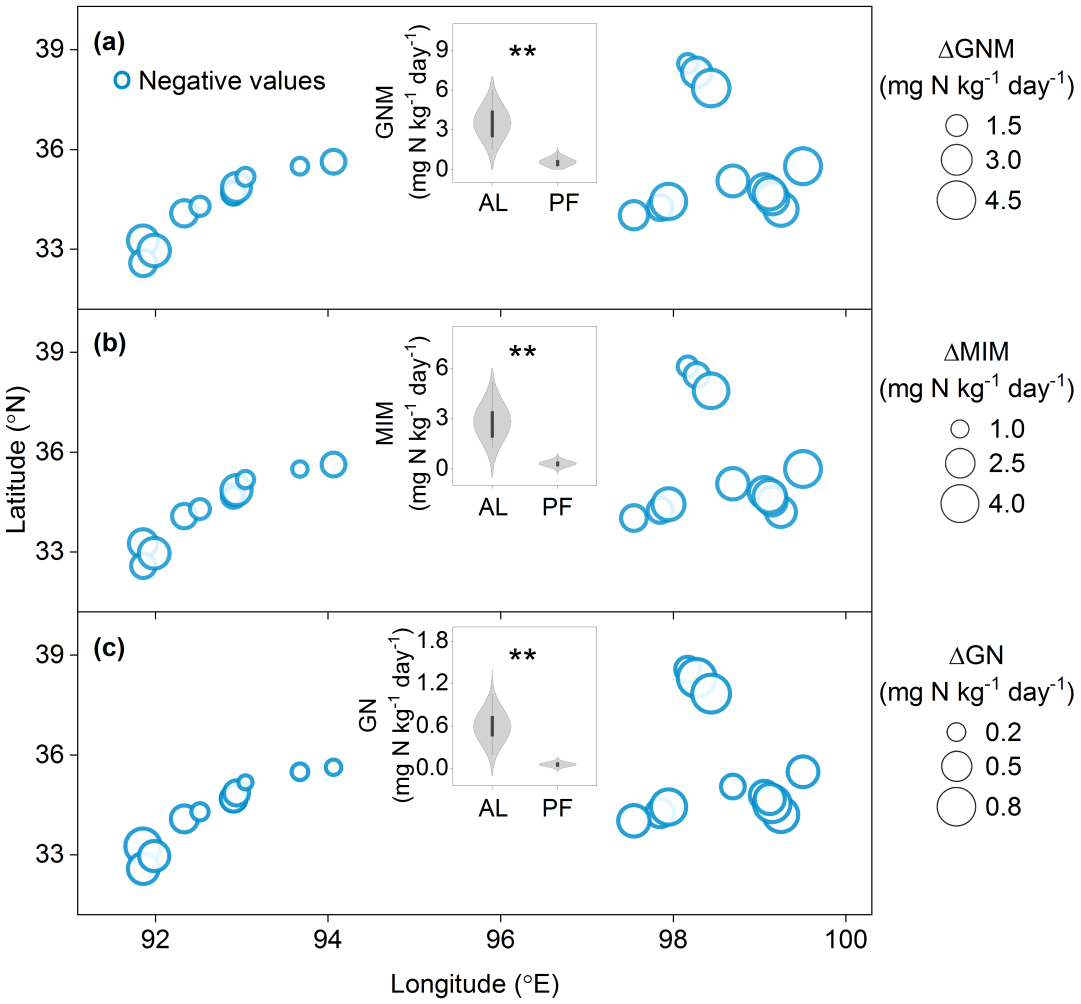

gcb_15205_f2.png

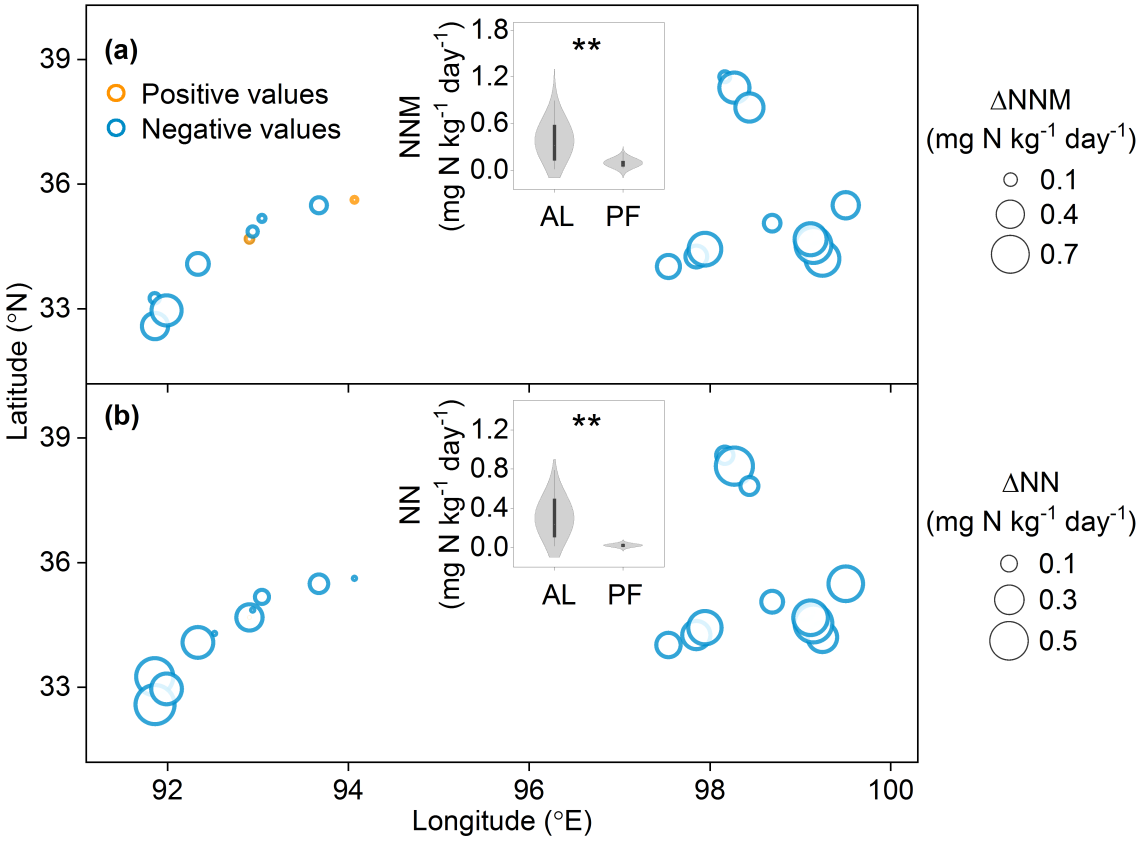

gcb_15205_f3.png

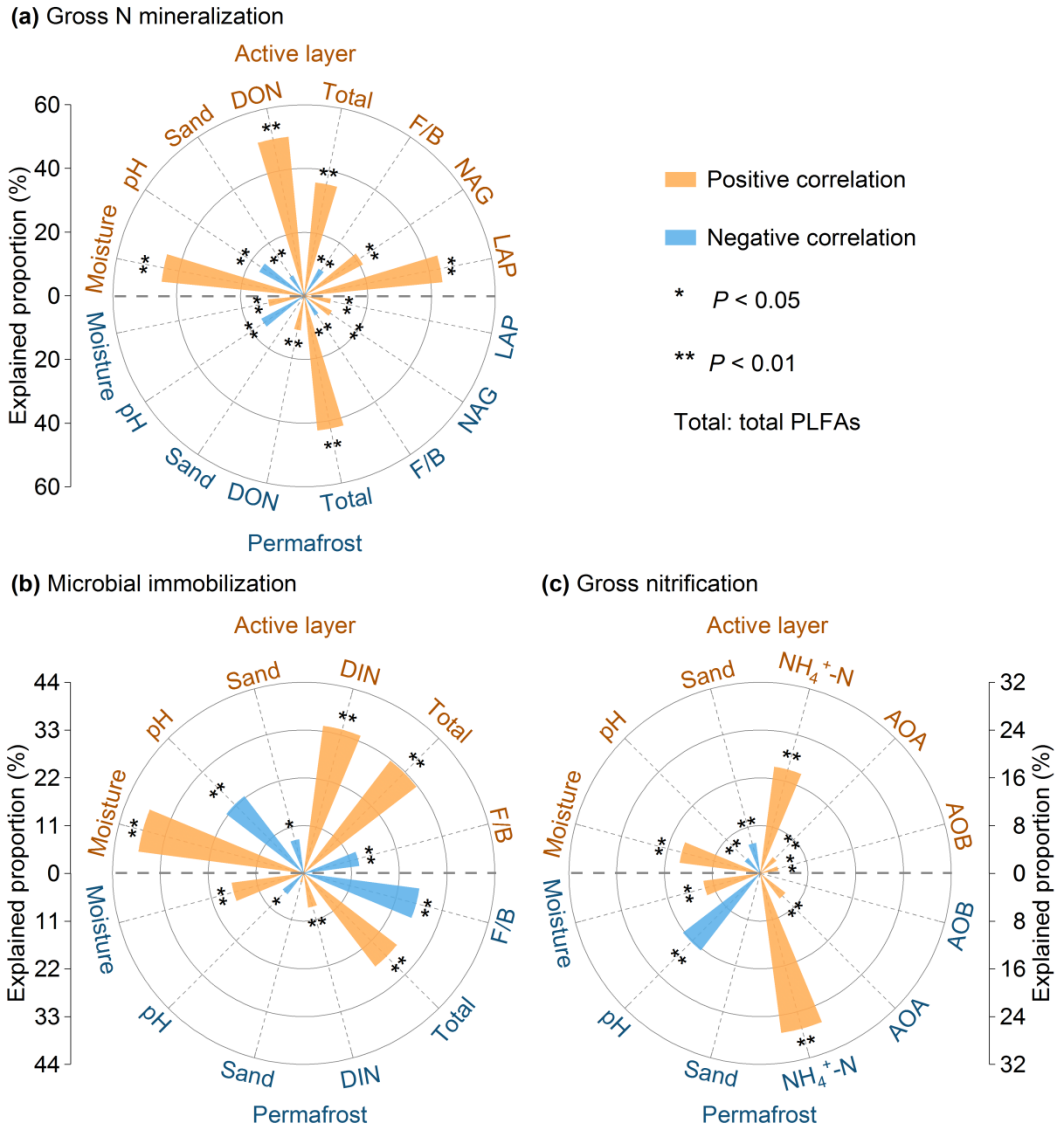

gcb_15205_f4.png

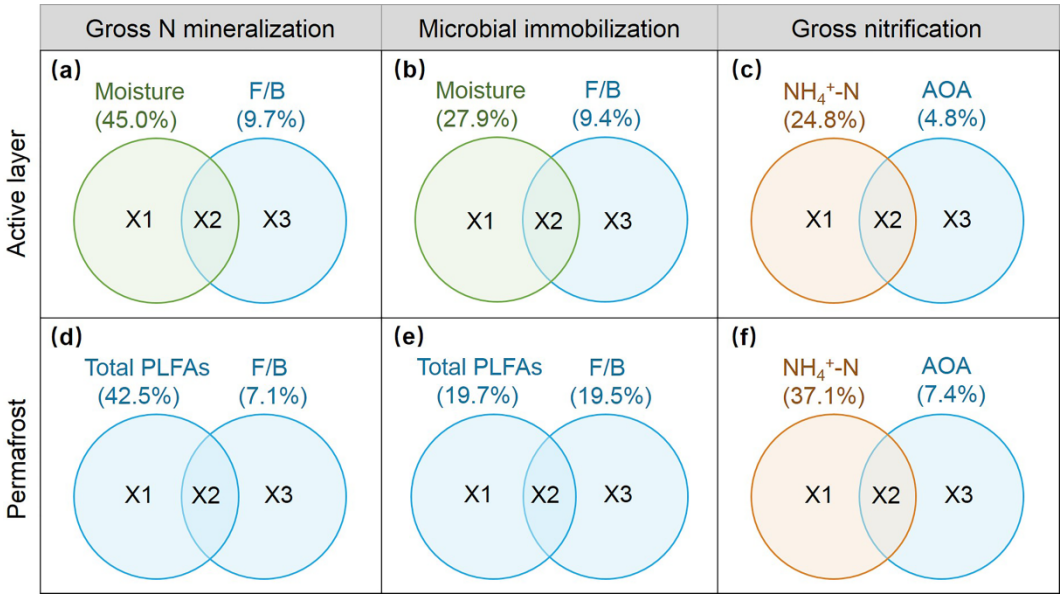

gcb_15205_f5.png

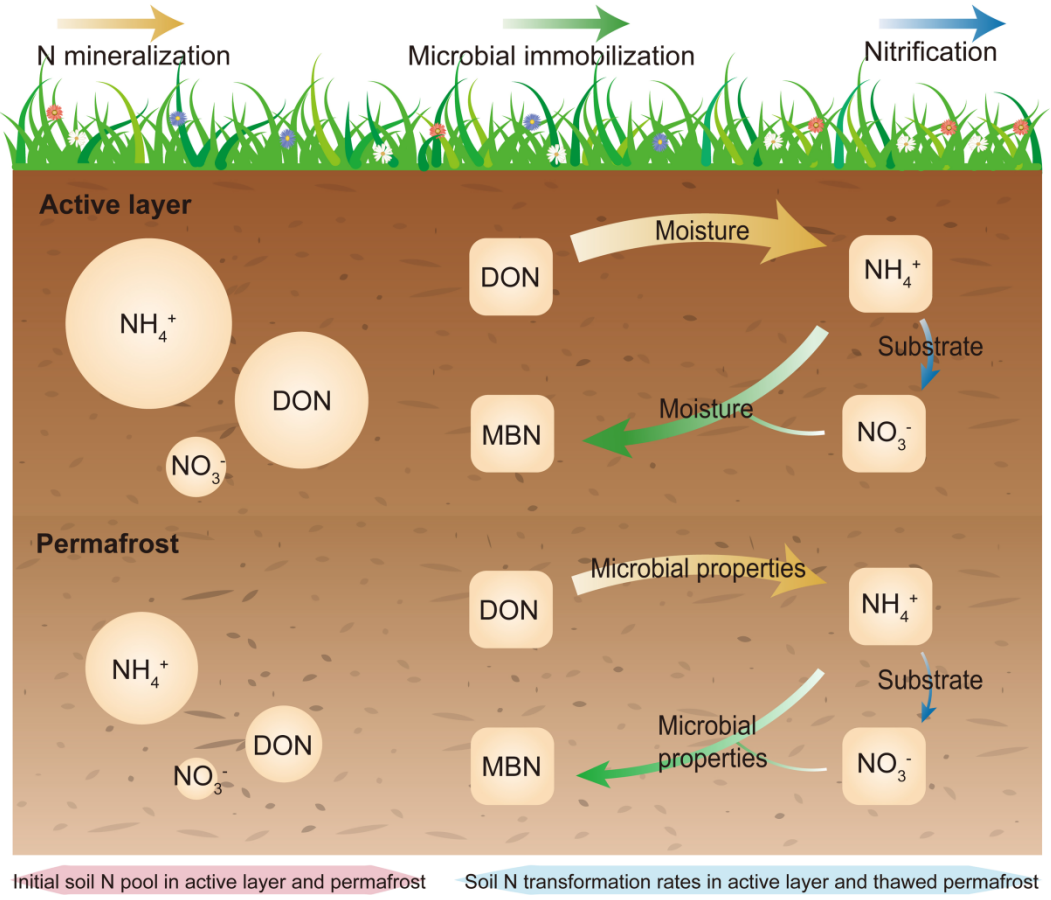

gcb_15205_f6.png